PROCEEDINGS OF SPIE

SPIEDigitalLibrary.org/conference-proceedings-of-spie

Spectral retrieval techniques for high-resolution Fourier-transform micro-spectrometers

Alaine Herrero-Bermello, Aitor V. Velasco, Hugh Podmore, Pavel Cheben, Jens H. Schmid, et al.

Alaine Herrero-Bermello, Aitor V. Velasco, Hugh Podmore, Pavel Cheben, Jens H. Schmid, Siegfried Janz, María L. Calvo, Dan-Xia Xu, Alan Scott, Regina Lee, "Spectral retrieval techniques for high-resolution Fourier-transform micro-spectrometers," Proc. SPIE 10683, Fiber Lasers and Glass Photonics: Materials through Applications, 1068319 (17 May 2018); doi: 10.1117/12.2306130

SPIE.

Event: SPIE Photonics Europe, 2018, Strasbourg, France

Spectral retrieval techniques for high-resolution Fourier-transform micro-spectrometers

Alaine Herrero-Bermello[1], Aitor V. Velasco*[1], Hugh Podmore[2], Pavel Cheben[3], Jens H. Schmid[3], Siegfried Janz[3], María L. Calvo[4], Dan-Xia Xu[3], Alan Scott[5], Regina Lee[2]

[1]Spanish National Research Council (CSIC), Madrid, Spain
[2]Department of Physics and Astronomy, York University, Toronto, ON, Canada
[3]National Research Council, Ottawa, ON, Canada
[4]Complutense University, Madrid, Spain
[5]Honeywell Aerospace, Kanata, ON, Canada
*a.villafranca@csic.es; phone +34 915618806; fax +34914117651

ABSTRACT

Spatial heterodyne Fourier transform (SHFT) spectroscopy is based on simultaneous interferometric measurements implementing linearly increasing optical path differences, hence circumventing the need for mechanical components of traditional Fourier transform spectroscopy schemes. By taking advantage of the high mode confinement of the Silicon-on-Insulator (SOI). platform, great interferometric lengths can be implemented in a reduced footprint, hence increasing the resolution of the device. However, as resolution increases, spectrometers become progressively more sensitive to environmental conditions, and new spectral retrieval techniques are required. In this work, we present several software techniques that enhance the operation of high-resolution SHFT micro-spectrometers. Firstly, we present two techniques for mitigating and correcting the effects of temperature drifts, based on a temperature-sensitive calibration and phase errors correction. Both techniques are demonstrated experimentally on a 32 Mach-Zehnder interferometers array fabricated in a Silicon-on-insulator chip with microphotonic spirals of linearly increasing length up to 3.779 cm. This configuration provides a resolution of 17 pm in a compact device footprint of 12 mm2. Secondly, we propose the application of compressive-sensing (CS) techniques to SHFT micro-spectrometers. By assuming spectrum sparsity, an undersampled discrete Fourier interferogram is inverted using l1-norm minimization to retrieve the input spectrum. We demonstrate this principle on a subwavelength-engineered SHFT with 32 MZIs and a 50 pm resolution. Correct retrieval of three sparse input signals was experimentally demonstrated using data from 14 or fewer MZIs and applying common CS reconstruction techniques to this data.

Keywords: SOI, Fourier transform, spectrometry

1. INTRODUCTION

1.1 Spatial-heterodyne Fourier Transform spectroscopy

Fourier-transform spectroscopy is a power analysis technique traditionally based on a Michelson interferometer with a moving mirror for a variable optical delay [1]. Spatial heterodyne Fourier-transform (SHFT) spectrometers circumvent the need of mechanical elements by performing multiple parallel measurements at fixed optical path length differences [2]. The source spectrum is calculated by Fourier transformation of the resulting stationary interference patterns. Since, SHFT configuration only requires passive elements, it can be implemented with planar waveguides achieving high spectral resolution in a compact device with reduced fabrication costs [3,4]. In particular, the high refractive index contrast of the silicon-on-insulator (SOI) platform results in a high mode confinement and a small bend radius that enables an increased spectral resolution in a reduced footprint [5-7]. Furthermore, integrated SHFT spectrometers advantageously benefit from the intrinsically large étendue of the Michelson interferometer [8] and the possibility of multiple input waveguide apertures [9], circumventing single-aperture input limitations of array waveguide gratings (AWGs) [10,11] and waveguide echelle gratings [10,12]. These features show remarkable potential for a broad range of applications such as biological and environmental sensing, genomics, health diagnostics, microsatellites or fiber optic telecommunication networks [13,14].

Fiber Lasers and Glass Photonics: Materials through Applications, edited by
Stefano Taccheo, Jacob I. Mackenzie, Maurizio Ferrari, Proc. of SPIE Vol. 10683
1068319 · © 2018 SPIE · CCC code: 0277-786X/18/$18 · doi: 10.1117/12.2306130

The SHFT scheme can be implemented in a SOI platform as an array of waveguide MZIs with linearly increasing optical path differences [5]. The number of interferometers (N) and the physical length difference of the most unbalanced interferometer (ΔL_{max}) determines the spectral resolution ($\delta\lambda$) and the free spectral range (FSR) of the device [9]:

$$\delta\lambda = \frac{{\lambda_0}^2}{\Delta L_{max} n_g} \tag{1}$$

$$FSR = \delta\lambda \frac{N}{2} \tag{2}$$

where λ_0 is the device operational central wavelength and n_g is the waveguide group index. For any arbitrary input signal, all the outputs of the device, corresponding to each interferometer, are measured simultaneously providing an output wavelength dependent spatial interferogram $I(x_i)$. The relation between the input spectral distribution B, and the output interferogram within the FSR of the device is determined by [9]:

$$I(x_i) = \int_0^{FSR} B(\bar{\sigma}) \cos(2\pi\bar{\sigma}x_i) d\bar{\sigma} \tag{3}$$

where $\bar{\sigma}$ is the shifted wavenumber, relative to the Littrow wavenumber σ_L, and x_i is the path delay of the i-th MZI. This relation is unambiguous for an ideal device without phase errors enabling the source spectrum to be retrieved by the cosine Fourier transform (FT). However, environmental fluctuations due thermal dependence of Si-wire waveguides [15], as well as fabrication deviations from ideal behavior, result in phase and amplitude errors which cause the non-orthogonality of the Fourier transform base. Compensation through either active elements [7] or data processing techniques are hence required to prevent errors in the spectral retrieval.

1.2 Spectral retrieval

Three main deviations from the ideal behavior must be taken into account during the data processing stage, namely phase errors, amplitude errors and thermal fluctuations. Amplitude errors are produced by uneven propagation losses along the waveguides, resulting in reduced visibility for more unbalanced MZIs which can nevertheless be readily compensated by normalization techniques. Phase errors are caused by small deviations in the chip fabrication process which induce alterations of the effective index and optical path differences. These variations prevent the verification of the Littrow wavenumber phase alignment condition, rendering Eq. 3 inadequate for spectral retrieval. A calibration-based spectral retrieval algorithm can be employed to overcome this issue [9,13]. According to this approach, the transmittance function of each MZI is sampled at M equidistant wavelengths within the FSR of the device resulting in a transformation matrix C. This matrix comprises N rows, which represent the normalized power of the output interferogram for each sampled wavelength, and M columns, which represent the spectral response of each MZI. Therefore, the relation between the input signal and the output interferogram is:

$$I(x_i) = B \times C \tag{4}$$

where B is the source power spectrum, C is the calibration matrix and I is the output interferogram. In the absence of phase errors, the transformation base is orthogonal and the calibration matrix invertible. In a real scenario, the source spectrum can be obtained multiplying the interferogram by the pseudoinverse of the transformation matrix.

However, in order for the proposed algorithm to work correctly, the MZIs transmittance functions must remain constant between the calibration process and the device operation. Si-wire waveguides thermal dependence hampers this conditions, as temperature changes modify the waveguide effective index and therefore the optical path difference of each interferometer and the period of the resulting transmittance function. At a wavelength of 1.55 μm, the thermooptic coefficients of the device waveguides are $1.8 \cdot 10^{-4}$ K^{-1} and $1.8 \cdot 10^{-4}$ $K^{-1}$and for TE and TM polarizations, respectively [15]. This thermal dependence is proportional to the maximum interferometric delay, therefore imposing harder conditions on the thermal stabilization system and ultimately limiting the maximum achievable resolution.

2. TEMPERATURE DEPENDENCE MITIGATION

2.1 Principle of operation

Two spectral retrieval techniques for software SHFT athermalization are presented [6]. The first proposed algorithm is based on a temperature-sensitive calibration in which multiple calibration matrices C_j are measured at different temperatures T_j. Therefore the output interferogram is determined by:

$$I(x_i, T_j, \lambda_k) = B(\lambda_k) \times C_j \quad (4)$$

where λ_k are equidistant wavelengths within the FSR of the device.

For a correct selection of the calibration matrix, an auxiliary temperature measurement is performed. This step can be directly implemented with a high precision measurement of the photonic chip temperature (T_{aux}). The calibration matrix at a temperature T_j closest to T_{aux} is subsequently selected for the spectral retrieval algorithm. Alternatively, the output interferogram I_{aux} of a reference input signal with a known spectrum B_{ref} can be used for accurate temperature determination. In this case, the appropriate calibration matrix is selected by minimizing the following expression:

$$\sum_{i=1}^{N} \left| I_{aux} - B_{ref} \times C_j \right| \quad (5)$$

Additionally, a second software athermalization technique for narrowband signals is reported. In this case, the phase errors in the calibration matrix are corrected by shifting and aligning the MZIs transmittance functions (Fig. 4) obtaining a phase shift vector $\Delta\varphi$. By verifying the phase alignment condition of Littrow wavenumber, a FT-based spectral retrieval can be used:

$$B(\lambda_k) = A \sum_{k=1}^{N} I'(k) \cos\left(\frac{\pi\, n\, k}{N}\right) \quad (6)$$

where A is a normalization constant, k is the number of points of the interferogram, n is the number of points of the spectrum and $I'(k)$ is a corrected interferogram by also applying phase shift vector $\Delta\varphi$.However, an indetermination arises when applying $\Delta\varphi$ to an output interferogram, as a given signal level can correspond to either a rising or descending flank of the MZI transmittance function. To solve this issue, the output interferogram is measured at two close temperatures T and $T+\Delta T$. By analyzing the effect of small temperature changes in the output signal levels, the indetermination is resolved and the phase shift vector can be applied correctly.

2.2 Experimental demonstration

The algorithms were experimentally demonstrated on a SHFT micro-spectrometer comprising an array of 32 silicon waveguide Mach-Zehnder interferometers with a reference straight arm of constant length and a microphotonic spiral arm of linearly increasing length (Fig. 1) [5]. The high-index contrast of the SOI platform enables fabrication of very tightly coiled spirals, achieving a maximum length difference of ΔL_{max}=3.779 cm in a spiral diameter of only 490 μm. These design parameters result in a spectral resolution of 17 pm and a FSR of 0.23 nm in a compact device footprint of 23 mm^2. To ensure monomode operation and minimize bend losses, 450 nm wide Si-wire waveguides with a minimum bend radius of 5 μm were used. The device was fabricated on SOI wafers with 0.26-μm- thick silicon and 2-μm- thick buried oxide. Si-wire waveguide structures were defined in a single patterning step by electron beam lithography using hydrogen silsesquioxane (HSQ) resist. Inductively coupled plasma reactive ion etching was used to transfer the resist pattern into the silicon layer.

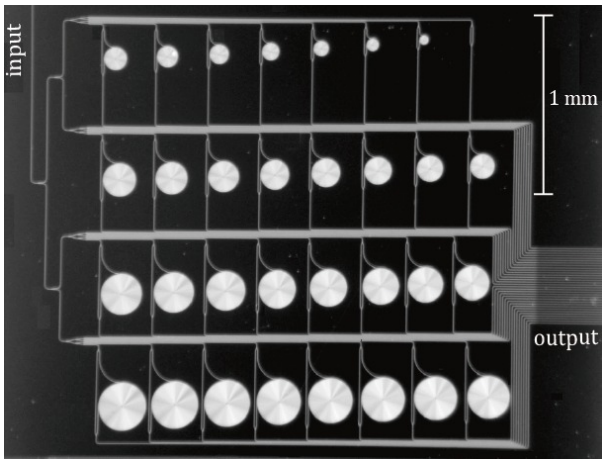

Figure 1. Optical micrograph of the fabricated spatial heterodyne Fourier-transform spectrometer chip with spiral silicon wire waveguides.

The fabricated device was characterized using a high-resolution tunable semiconductor laser over the spectral range of 1550-1550.6 nm, with a wavelength step of 0.5 pm. Efficient subwavelength grating couplers [16] were included at the input and output facets of the chip for optimized fiber coupling, while at the same time reducing the Fabry-Perot effect due to the reflectivity at the facets. A Peltier stage was used for thermal stabilization of the chip, and TM-polarized input field was selected through an external polarization controller. Output light from all the MZIs was collected in a single shot with a high-sensitivity IR CCD camera.

2.3 Spectral retrieval results

Figure 2 presents an experimental spectral retrieval of a monochromatic signal after selecting the appropriate calibration matrix, as well as the effects of a temperature mismatch in said retrieval. In the absence of proper correction, thermal drifts affect each MZI differently depending on its optical path difference, and the retrieved spectrum is not only shifted, but also deformed by the presence of artifacts. In particular, a 6 pm central-wavelength displacement is measured for a 0.1 ºC mismatch, whereas the spectrum deterioration is already significant for a temperature variation of 0.3 °C. When compensated through multi-temperature calibration and phase alignment, spectrum is correctly retrieved even in a device with a resolution as high as 17 pm.

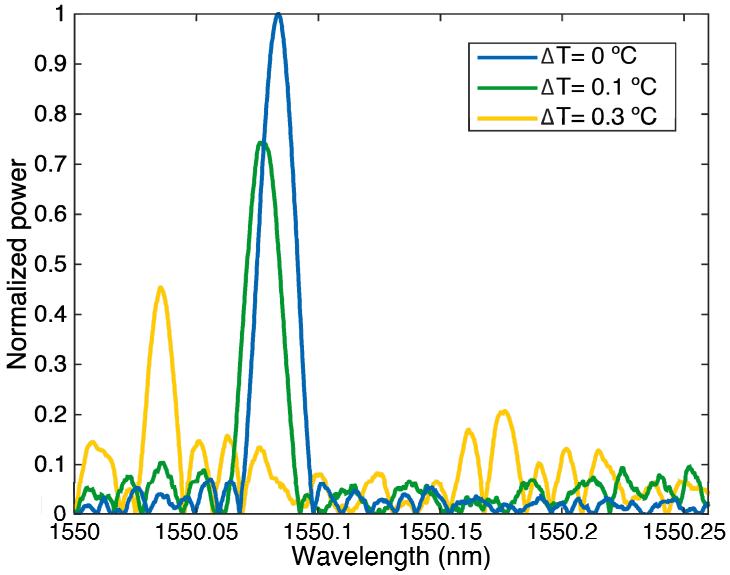

Figure 2. Spectral retrieval of a monochromatic input signal for different temperature changes between the calibration and measurement steps.

3. COMPRESSIVE SENSING

3.1 Principle of operation

Spectral retrieval techniques based on compressive-sensing (CS) principles [17] are also presented. In a CS scheme, the assumption of a sparse input signal leads to a reduction in the number of sampling points required to correctly retrieve the input signal. CS techniques are particularly suitable for SHFT devices as sampling points in the interferogram are collected independently and the sensing basis (frequency) and the measurement basis (temporal) are maximally incoherent, meaning that a sparse signal in the frequency domain will produce a non-zero signal level at all points in the time-domain. By inverting an undersampled interferogram through l1-norm minimization, spectra can be retrieved using a lesser number of MZI without loss of information.

3.2 Experimental demonstration

SHFT compressive sensing retrieval was demonstrated on an array of 32 MZI interferometers with refractive index engineering through subwavelength gratings (SWG) [18], schematically depicted in figure 3. SWG are periodical dispositions of alternating core and cladding slabs, with a smaller spacing than the wavelength of the propagated light. This structure acts as an optical metamaterial with a propagation constant that is controlled by the periodicity and the

duty-cycle of the grating [19]. Each MZI of the fabricated device comprises a first arm with a Si-wire waveguide (width 450 nm) and a second arm with a SWG section (width 300 nm, grating periodicity 400 nm, 50% grating fill-factor). This results in a group index of the subwavelength region of n_{SWG}=1.51, and a group index for the wire waveguide region of n_{WG}=4.38. A maximum SWG length of 1.5 cm results in a total resolution of 48 pm and a FSR of 0.78 nm.

The MZIs were fabricated on a wafer consisting of a Si substrate, buried oxide layer, a 260 nm thick Si layer from which waveguides are formed, and an SU-8 upper cladding. A high-resolution tuneable laser source was used to characterize the response of the subwavelength waveguide spectrometer. The excitation wavelength was steadily incremented in 5 pm steps over the FSR of the device, while the input power was held constant at 1mW. The input light was restricted to the transverse magnetic polarization state (TM), and coupled to the spectrometer via a lensed fiber.

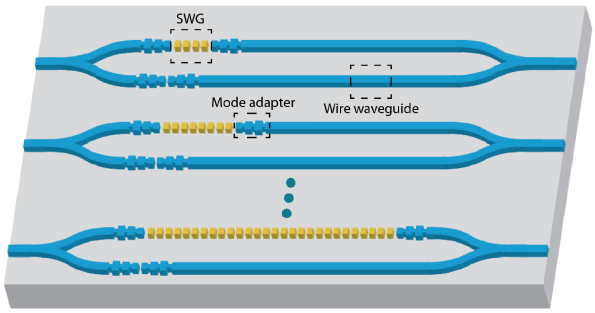

Figure 3. Schematic representation of the SWG-based spatial-heterodyne Fourier-Transform microspectrometer used for CS retrieval demonstration.

3.3 Spectral retrieval results

Figure 4 presents an experimental spectral retrieval of a monochromatic signal generated by a narrow-band laser centered at 1550.5 nm. For CS reconstruction demonstration, 8 MZIs are selected randomly from the instrument set, their output values are recorded, and the input spectrum is retrieved through l1-norm minimization via basis-pursuit denoising [20]. These results are compared with retrievals obtained using the pseudoinverse of the calibration map, both using the full MZI array, and the equivalent undersampled interferogram used for CS-reconstruction. These results show that spectrum is correctly retrieved by CS-based techniques even in an undersampled scenario where traditional approaches fail to appropriately characterize the input signal. Note that the narrow appearance of the spectral features in CS-reconstruction do not imply a higher spectral resolution, being instead a straightforward consequence of the initial sparsity assumption of the CS methods.

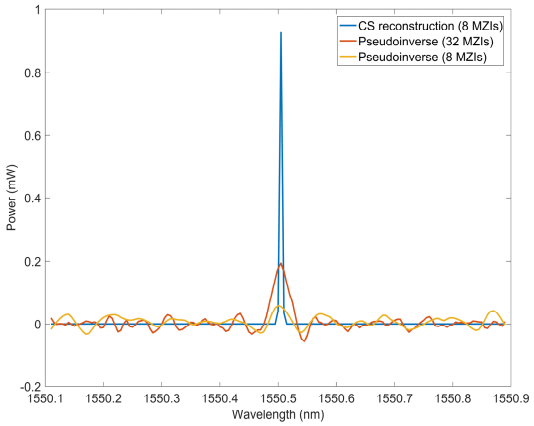

Figure 4. Spectra from narrow-band laser source with 1 mW input power retrieved via l1-norm minimization using a subset of 8 MZIs randomly selected (blue), via pseudoinverse methods with the full MZI array (orange), and via pseudoinverse with undersampled interferogram (yellow).

4. CONCLUSIONS

We have presented several spectral retrieval techniques for enhanced operation of spatial heterodyne Fourier-transform microspectrometers. Firstly, thermal drifts have been mitigated through multi-temperture calibration and phase alignment. This approach was demonstrated in a device of 17 pm resolution implemented with an array of 32 silicon waveguide Mach-Zehnder interferometers with SOI micro-photonic spirals. Secondly, a compressive sensing technique has been proposed for SHFT devices, enabling downsampled spectral retrieval without resolution or accuracy loss. This principle was demonstrated on a photonic chip consisting of 32 subwavelength-engineered MZIs with a resolution of 50 pm.

The combination of both techniques paves the way for high-resolution microspectrometers with a compact footprint and enhanced resilience to environmental fluctuation. Resulting miniaturized SHFT devices would be of paramount interest in diverse fields such as biological and environmental sensing, health diagnostics or microsatellites, and particularly, for the measurement of naturally occurring sparse signals, such as Raman and LIBS emission spectra, and atmospheric absorption and emission spectra.

ACKNOWLEDGEMENTS

We acknowledge the support from the National Research Council Canada, the Canadian Space Agency (CSA), and the Natural Sciences and Engineering Research Council of Canada (NSERC), by the Spanish “Ministerio de Economía y Competitividad” through projects TEC2015-71127-C2-1-R and TEC2015-71127-C2-2-R, by the “Comunidad de Madrid” through program SINFOTON-CM S2013/MIT-2790, and EURAMET through projects JRP-i22 14IND13 Photind and project 734331-H2020-MSCA-RISE:SENSIBLE. The EMRP is jointly funded by the EMRP participating countries within EURAMET and the European Union. This work was also supported in part by the EMPIR initiative, which is co-funded by the European Union's Horizon 2020 research and innovation programme and the EMPIR Participating States. Aitor V. Velasco acknowledges support from "Ministerio de Economía y Competitividad" through grant FJCI-2014-22836.

REFERENCES

[1] R. Bell, Introductory Fourier transform spectroscopy. Elsevier, 2012.

[2] J. M. Harlander, F. L. Roesler, J. G. Cardon, C. R. Englert and R. R. Conway, "A Spatial Heterodyne Spectrometer for Remote Sensing of Earth's Middle Atmosphere," *Appl. Opt*., vol. 41, no. 7, pp. 1343-1352,. 2002.
[3] P. Cheben, I. Powell, S. Janz and D.-X. Xu, "Wavelength-dispersive device based on a Fourier-transform Michelson-type arrayed waveguide grating," *Opt. Lett.,* vol 30, no. 14, pp. 1824-1826, July 2005.
[4] M. Florjańczyk, P. Cheben, S. Janz, A. Scott, B. Solheim and D.-X. Xu, "Multiaperture planar waveguide spectrometer formed by arrayed Mach-Zehnder ineterferometers," *Opt. Express,* vol 15, no. 26, pp. 18176-18189, Dec. 2007.
[5] A. V. Velasco, P. Cheben, P. J. Bock, A. Delâge, J. H. Schmid, J. Lapointe, S. Janz, M. L. Calvo, D.-X. Xu, M. Florjańczyk and M. Vachon, "High-resolution Fourier-transform spectrometer chip with microphotonic silicon spiral waveguides," *Opt. Lett., vol.* 38, no. 5, pp. 706-708, Mar. 2013.
[6] A. Herrero-Bermello, A. V. Velasco, H. Podmore, P. Cheben, J. H. Schmid, S. Janz, M. L. Calvo, D.-X. Xu, A. Scott and P. Corredera, "Temperature dependence mitigation in stationary Fourier-transform on-chip spectrometers," *Opt. Lett.* vol. 42, no. 11, pp. 2239-2242, Jun 2017.
[7] K. Okamoto, H. Aoyagi and D. Takada, "Fabrication of Fourier-transform, integrated-optic spatial heterodyne spectrometer on silica-based planar waveguide," *Opt. Lett.*, vol. 35, no. 12, pp 2103-2015, June 2010.
[8] P. Jacquinot, "The Luminosity of Spectrometers with Prisms, Gratings, or Fabry-Perot Etalons," J. Opt. Soc. Am., vol. 44, no. 10, pp. 761-765, Oct. 1954.
[9] A. V. Velasco, P. Cheben. M. Florjańczyk and M. L. Calvo, "Spatial Heterodyne Fourier-Transform Waveguide Spectrometers," in *Progress in Optics*, E. Wolf. Ed. Elsevier: Oxford, 2014, pp. 159-205.
[10] P. Cheben, "Wavelength dispersive planar waveguide devices: echelle gratings and arrayed waveguide gratings," in *Optical Waveguides: from Theory to Applied Technologies*, M. L. Calvo and V. Laksminarayanan. Ed. CRC: New York, 2007, pp. 173-230.
[11] P. Cheben, J. H. Schmid, A. Delâge, A. Densmore, S. Janz, B. Lamontagne, J. Lapointe, E. Post, P. Waldron and D.-X. Xu, "A high-resolution silicon-on-insulator arrayed waveguide grating microspectrometer with sub-micrometer aperture waveguides," *Opt. Express,* vol. 15, no. 5, pp. 2299-2306, Mar. 2007.
[12] S. Janz, A. Balakrishnan, S. Charbonneau, P. Cheben, M. Cloutier, A. Delâge, K. Dossou, L. Erickson, M. Gao, P. A. Krug, B. Lamontagne, M. Packirisamy, M. Pearson and D.-X. Xu, "Planar waveguide echelle gratings in silica-on-silicon," IEEE Photon. Technol. Lett., vol. 16, no. 2, pp. 503-505, Feb. 2004.
[13] C. P. Bacon, Y. Mattley and R. DeFrece, "Miniature spectroscopic instrumentation: applications to biology and chemistry," *Rev. Sci. Instrum.*, vol. 75, no. 1, pp 1–16, 2004.
[14] J. Blacksberg, E. Alerstam, Y. Maruyama, C. J. Cochrane, and G. R. Rossman, "Miniaturized time-resolved raman spectrometer for planetary science based on a fast single photon avalanche diode detector array," *Appl. Opt.*, vol. 55, no. 4, pp. 739–748, Feb 2016.
[15] J. H. Schmid, M. Ibrahim, P. Cheben, J. Lapointe, S. Janz, P. J. Bock, A. Densmore, B. Lamontagne, R. Ma, W. N. Ye and D.-X. Xu, "Temperature- independent silicon wavelength grating waveguides," *Opt. Lett*., vol. 36, no. 11, pp. 2110-2112, June 2011.
[16] P. Cheben, P. J. Bock, J. H. Schmid, J. Lapointe, S. Janz, D.-X. Xu, A. Densmore, A. Delâge, B. Lamontagne, and T. J. Hall, "Refractive index engineering with subwavelength gratings for efficient microphotonic couplers and planar waveguide multiplexers," *Opt. Lett*., vol. 35, no. 15, pp. 2526-2528, Aug. 2010.
[17] E. J. Candes and M. B. Wakin, "An introduction to compressive sampling," *IEEE Signal Process Mag.*, vol. 25, no. 2, pp. 21–30, March 2008.
[18] H. Podmore, A. Scott, P. Cheben, A. V. Velasco, J. H. Schmid, M. Vachon, and R. Lee, "Demonstration of a compressive-sensing Fourier-transform on-chip spectrometer," *Opt. Lett.* vol. 42, no. 7, pp. 1440-1443, Apr 2017.
[19] P. J. Bock, P. Cheben, A. V. Velasco, J. H. Schmid, A. Delage, M. Florjanczyk, J. Lapointe, D.-X. Xu, M. Vachon, S. Janz, and M. L. Calvo "Subwavelength grating fourier-transform interferometer array in silicon-on-insulator," *Laser Photonics Rev*., vol. 7, no. 6, pp. L67–L70, 2013.
[20] E. van den Berg and M. P. Friedlander, "Probing the pareto frontier for basis pursuit solutions," *SIAM J. Sci. Comput.* vol. 31, no. 2, pp. 890–912, 2008.